Equivalence of position-position auto-correlations in the Slicer Map and the Lévy-Lorentz gas

C. Giberti[(a)], L. Rondoni[(b,c)], M. Tayyab[(b,d)] and J. Vollmer[(b,e)]

[(a)] Dipartimento di Scienze e Metodi dell'Ingegneria, Università di Modena e Reggio E., Via Amendola 2, Padiglione Morselli, I-42122 Reggio E., Italy

[(b)] Dipartimento di Scienze Matematiche, Giuseppe Luigi Lagrange, Politecnico di Torino, Corso Duca degli Abruzzi 24 I-10129 Torino, Italy

[(c)] Present address: Civil and Environmental Engineering Department, and Princeton Environmental Institute, Princeton University, 59 Olden St, Princeton, NJ 08540, USA

[(d)] Dipartimento di Matematica, Giuseppe Peano, Università degli Studi di Torino, Via Carlo Alberto 10, I-10123 Torino, Italy

[(e)] Present address: Institut für Theoretische Physik, Universität Leipzig, Brüderstr. 16, D-04103 Leipzig, Germany

April 1, 2019

Abstract

The Slicer Map is a one-dimensional non-chaotic dynamical system that shows sub-, super-, and normal diffusion as a function of its control parameter. In a recent paper [Salari et al., CHAOS 25, 073113 (2015)] it was found that the moments of the position distributions as the Slicer Map have the same asymptotic behaviour as the Lévy-Lorentz gas, a random walk on the line in which the scatterers are randomly distributed according to a Lévy-stable probability distribution. Here we derive analytic expressions for the position-position correlations of the Slicer Map and, on the ground of this result, we formulate some conjectures about the asymptotic behaviour of position-position correlations of the Lévy-Lorentz gas, for which the information in the literature is minimal. The numerically estimated position-position correlations of the Lévy-Lorentz show a remarkable agreement with the conjectured asymptotic scaling.

Keywords: Slicer Map, Lévy-Lorentz lattice gas, position-position auto-correlation function, anomalous transport.

1 Introduction

One object of interest in studies of anomalous transport is the *transport exponent* γ (Klages et al., 2008):

$$\gamma := \lim_{n\to\infty} \frac{\log\langle \Delta \mathbf{x}_n^2 \rangle}{\log n}\,, \tag{1}$$

where $\langle \Delta \mathbf{x}_n^2 \rangle$ is the mean-square displacement of the positions at time n. Regimes with $\gamma < 1$ are called sub-diffusion; they are called diffusion if $\gamma = 1$, and super-diffusion if $\gamma > 1$. Some special cases treated in Salari et al. (2015), such as logarithmic growth of $\langle \Delta \mathbf{x}_n^2 \rangle$, are not described by Eq. (1), which merely yields $\gamma = 0$, *cf.* Theorem 6. However, when Eq. (1) holds with $\gamma > 0$ the generalised diffusion coefficient D_γ, defined by:

$$D_\gamma := \lim_{n\to\infty} \frac{\langle \Delta \mathbf{x}_n^2 \rangle}{n^\gamma}\,, \tag{2}$$

exists and is a non-negative number.

Transport properties afford only a rather coarse representation of the typically very rich underlying microscopic dynamics. Understanding them from a microscopic perspective is an open problem, that motivates a wide and very active research community (Klafter et al., 2012; Klages, 2007; Collet et al., 2005; Klages et al., 2008; Jepps et al., 2003; Sokolov, 2012). In the realm of deterministic dynamics, it is understood that uniformly hyperbolic dynamical systems produce rapid correlations decay. In turn, rapid decay of correlations is commonly associated with standard diffusion (Gaspard, 2005; Klages, 2007). Because randomly placed non-overlapping wind-trees[1] and related maps (Dettmann and Cohen, 2000; Cecconi et al., 2003) enjoy a sort of stochasticity analogous to that generated by chaotic dynamics, they may also show standard diffusion.

On the contrary, for fully deterministic systems with vanishing Lyapunov exponents, such as systems of point particles within periodic polygonal walls (Jepps and Rondoni, 2006), the nature of transport is still a matter of investigation (Zaslavsky, 2002; Klages, 2007; Klages et al., 2008; Salari et al., 2015). A major challenge of the latter systems is that correlations persist or decay rather slowly as compared to what happens in chaotic systems (Jepps and Rondoni, 2006). This makes their asymptotic statistics much harder to understand than in the presence of chaos. Indeed, the unpredictability of single trajectories in strongly chaotic systems, like axiom A systems, that is one aspect of the fast decay of correlations, is often associated with regular behaviour on the level of ensembles, as proven, for instance, by the differentiability of SRB states (Ruelle, 1997) that implies linear response (Ruelle, 1998). In contrast, for non-chaotic systems the parameter dependence of the transport exponent can be quite irregular (Jepps and Rondoni, 2006). (Generalized) diffusion coefficients may be irregular even in chaotic systems (Klages, 2007).

In the field of fully fledged stochastic processes, numerous questions remain open as well (Zaslavsky, 2002; Klages, 2007; Denisov et al., 2003; Li et al., 2005; Sokolov, 2012). Among such systems, the Lévy-Lorentz gas (LLg), a random walk in random environments, in which the scatterers are randomly distributed on a line according to a Lévy-stable probability distribution, has been thoroughly investigated by various authors. Different types of anomalous and standard diffusion were observed, upon tuning the parameter β characterising the Lévy-stable probability distribution (Barkai and Fleurov, 1999; Barkai et al., 2000). These authors noted that ballistic contributions to the mean-square displacement, which are considered irrelevant when diffusion is normal, are in fact important for the transport. Under certain simplifying assumptions, Burioni et al. (2010) analytically calculated the mean-square displacement of the travelled distance for this model, and numerically verified the validity of their reasoning. More recently, Bianchi et al. (2016) rigorously established the validity of the Central Limit Theorem.

The Slicer Map (SM) introduced in Salari et al. (2015) was motivated by observations of the mass transport of periodic polygonal billiards (Jepps and Rondoni, 2006). Like in polygonal billiards, the dynamics of the SM are free of randomness. Their trajectories do not separate exponentially in time, and they experience sudden deviations from their motion, at isolated points that are regularly placed in space. Despite these facts, the dynamics of the SM differs substantially from all other models mentioned so far. For instance, after an initial transient all trajectories of the SM turn periodic. However, anomalous transport may be dominated by ballistic flights (Aghion et al., 2017). Indeed the SM features anomalous transport because the length of ballistic flights in the initial ensemble follows a power-law distribution. Its transport exponent γ_α can be tuned by adjusting its parameter α that governs the power-law distribution of the ballistic flights.

Salari et al. (2015) showed that once α is adjusted so that the transport exponent of the SM coincides with that of the LLg at a given β, all higher order moments of the position distribution of the SM scale in time like those of the LLg (Burioni et al., 2010). Of course such an agreement does not imply a full equivalence of the dynamics, as mentioned above and further stressed in Sec. 2 and 4. For instance, from the particle-transport viewpoint, the

[1] In wind-tree models a "wind" particle moves with constant velocity on a plane, where it is elastically reflected at fixed square scatterers, the "trees".

LLg can only be super-diffusive ($1 < \gamma_\beta < 2$), while the SM can exhibit all possible diffusion regimes, $0 \leq \gamma_\alpha \leq 2$. Moreover, the β-dependence of the transport exponent of the LLg is not simple: it splits in three different functional forms. In contrast, $\gamma_\alpha = 2 - \alpha$ for all SM regimes.

The agreement of the moments of the displacement suggest an equivalence of the transport characteristics of the SM and the LLg. This is similar to findings in statistical physics, where systems with different microscopic dynamics can also share the same thermodynamic properties (*i.e.* averages and variances) and corresponding correlation functions. Nevertheless, such a correspondence is far from trivial. In particular for a transient, far-from equilibrium dynamics with non-normal diffusion a direct investigation is indispensible. The common wisdom is that it should be possible to identify differences in *some* correlation functions (Klages et al., 2008; Sokolov, 2012).

Here, we derive analytic expressions for the position-position auto-correlations of the SM, and we explore whether they suffice to distinguish its transport properties from those of the LLg and a closely related systems, the modified Lévy-Lorentz gas (LLg^+), that will be introduced in Sec. 3. As information on the position correlations of the LLg and the LLg^+ is minimal in the literature, we resort to numerical simulations to compare the SM with the LLg and the LLg^+. We find that the equivalence of the positions moments extends to the case of the position-position auto-correlation functions; for $1.5 \lesssim \gamma < 2$ their functional forms have been numerically found to match without adjustable parameters. Therefore, even these auto-correlations do not distinguish the Slicer Map and the (modified) Lévy-Lorentz gas.

This paper is organised as follows: Section 2 formally introduces the SM and summarises its main properties. They are derived here in an alternative fashion, compared to that of Salari et al. (2015). Some examples of the SM position auto-correlation functions are explicitly computed in Sec. 2.3. The correspondence between the LLg^+ and the SM is discussed in Sec. 3. The position-position auto-correlations of the SM and the LLg^+ are compared in Sec. 3.3. More precisely, leveraging on the knowledge of position-position auto-correlations of the SM, we propose some conjectures for the asymptotic scaling of the correlations of the LLg^+ and provide numerical evidence supporting them. In Sec. 4 we conclude the paper with a discussion of our main result: In the strongly super-diffusive regime, $1.5 \lesssim \gamma < 2$, the position-position auto-correlations of the SM and of the LLg^+ scale in the same fashion with time. We interpret this finding in terms of the distribution of the length of ballistic flights, which do not strongly depend on the details of the dynamics. For $1 \lesssim \gamma < 1.5$, good statistic is harder to obtain; we expect the equivalence to hold also in this parameter range, but at the moment we cannot properly support this expectation. Some technical points of the proof, that concern the time asymptotics of the moments and the auto-correlation function, are provided in an appendix.

2 The Slicer Map

To define the SM we introduce the fundamental space unit $M := [0, 1]$, consisting of the interval of positions. Replicating M in a one dimensional lattice, we produce the infinite configuration space: $\widehat{M} := M \times \mathbb{Z}$. Each of its cells is identified by an index $m \in \mathbb{Z}$: $\widehat{M}_m := [0, 1] \times \{m\}$. Every cell $\widehat{M}_m$ contains two *"slicers"*, $\{\ell_m\} \times \{m\}$ and $\{1 - \ell_m\} \times \{m\}$, with $0 < \ell_m < 1/2$. The slicers split each half of $\widehat{M}_m$ into two parts. Salari et al. (2015) parameterised the value of ℓ_m by a positive number α as follows:

$$\ell_m(\alpha) = \frac{1}{\left(|m| + 2^{1/\alpha}\right)^\alpha}, \qquad \text{with} \quad m \in \mathbb{Z}, \quad \alpha > 0\,. \tag{3}$$

The SM, $S_\alpha : \widehat{M} \to \widehat{M}$, is then defined on the configuration space $\widehat{M} := [0, 1] \times \mathbb{Z}$ as follows:

$$S_\alpha(x, m) = \begin{cases} (x, m-1) & \text{for} \quad 0 \leq x \leq \ell_m \text{ or } \frac{1}{2} < x \leq 1 - \ell_m, \\ (x, m+1) & \text{for} \quad \ell_m < x \leq \frac{1}{2} \text{ or } 1 - \ell_m < x \leq 1. \end{cases} \tag{4}$$

The map is neither injective nor surjective. It is nevertheless possible to define the inverse map when restricting to trajectories with initial conditions in cell $\widehat{M}_0$ (Salari et al., 2015).

The space $\widehat{M}$ can be endowed with a density of points that evolves under the action of S_α. In particular, we consider the initial density $\hat{\mu} := \lambda \times \delta_0$ on $\widehat{M}$, where λ is the Lebesgue measure on M and δ_0 is the Dirac measure on the integer 0. Then, S_α can be interpreted as describing the transport of non-interacting particles in a one-dimensional space.[2]

Let $\pi_{[0,1]}$ and $\pi_{\mathbb{Z}}$ be the projections of $\widehat{M}$ on its first and second factors, respectively. Taking $x \in [0,1]$ and $m \in \mathbb{Z}$, we denote by $\hat{\mathbf{x}} = (x, m)$ a point in $\widehat{M}$, so that $\pi_{[0,1]}\hat{\mathbf{x}} = x$ and $\pi_{\mathbb{Z}}\hat{\mathbf{x}} = m$. Following Salari et al. (2015) we restrict our considerations to the initial distribution $\hat{\mu}$. We view $\widehat{M}$ as subdivided in two halves that are invariant for the SM: $\widehat{M}^+ := ([1/2,1] \times \{0\}) \cup ([0,1] \times \mathbb{Z}^+)$ and $\widehat{M}^- := ([0,1/2) \times \{0\}) \cup ([0,1] \times \mathbb{Z}^-)$. The dynamics in the two intervals are the mirror images of each other. Indeed, since at $m = 0$ the two slicers coincide with the single $\ell_0 = 1/2$, *cf.* Eq. (3), the points that lie initially in $[1/2, 1]$ never reach negative m, and those initially in $[0, 1/2)$ never reach positive m. Therefore, without loss of generality we restrict the following analysis to the positive part of the chain, $\widehat{M}^+$. The sequence of integers $\pi_{\mathbb{Z}}(S^j(\hat{\mathbf{x}}))$, $j \in \mathbb{N}$, will be called the *coarse-grained trajectory* of $\hat{\mathbf{x}}$. The distance travelled by $\hat{\mathbf{x}} = (x, 0)$ at time n will be denoted $\Delta\hat{\mathbf{x}}_n$.

A crucial aspect of the dynamics S_α is that its trajectories do not separate exponentially in time. Indeed different trajectories in $\widehat{M}$ neither converge nor diverge from each other in time, except when (in a discrete set of points) they are separated by a slicer, and their distance jumps discontinuously.

2.1 Mean Maximum Displacement and Maximum Square Displacement

To illustrate some fundamental properties of the slicer dynamics, let us introduce the symbols

$$\ell_m^+(\alpha) := 1 - \ell_m(\alpha) = 1 - \frac{1}{(m + 2^{1/\alpha})^\alpha} \qquad \text{with} \quad m \in \mathbb{N} \cup \{0\}\,. \tag{5}$$

They obey

$$\frac{1}{2} = \ell_0^+(\alpha) < \ell_1^+(\alpha) < \cdots < \ell_k^+(\alpha) < \ell_{k+1}^+(\alpha) < \cdots < 1, \quad \text{and} \quad \lim_{k\to\infty} \ell_k^+(\alpha) = 1\,. \tag{6}$$

Hence, there is a unique natural number $\overline{m} = \overline{m}_\alpha(x) > 0$ for any $x \in [1/2, 1)$ such that

$$\ell_{\overline{m}-1}^+(\alpha) < x \le \ell_{\overline{m}}^+(\alpha)\,. \tag{7}$$

In other words:

$$\overline{m}_\alpha(x) = \min\{m \in \mathbb{N} : \ell_m^+(\alpha) \ge x\} \quad \text{for } x \in [1/2, 1)\,. \tag{8}$$

Inspection of Eq. (4) and the definition (5) reveals that $\overline{m}_\alpha(x)$ is the maximum travelled distance for trajectories starting in the interval, Eq. (7):

Lemma 1: *Given $x \in [1/2, 1)$, let $\overline{m}(x)$ be the integer that satisfies Eq. (7). Then,*

$$S_\alpha(x, \overline{m}_\alpha(x)) = (x, \overline{m}_\alpha(x) - 1), \qquad S_\alpha(x, \overline{m}_\alpha(x) - 1) = (x, \overline{m}_\alpha(x)). \tag{9}$$

[2] The "particles" are the points moved by S_α. Analogously to the particles of systems such as the Ehrenfest gas, they do not interact with each other, since there is no coupling term connecting various particles in their equations of motion.

Proof. This is a straightforward consequence of Eqs. (4) and (7). □

This means that all trajectories become periodic with period 2 after the number $\overline{m}_\alpha(x)$ of steps. The description of the trajectory $\{S^j_\alpha(\hat{\mathtt{x}})\}_{j=0}^\infty$ with initial condition $\hat{\mathtt{x}} \in \widehat{M}_0$ is completed by the following Proposition.

Proposition 2: *For $x \in [1/2, 1)$, let $\hat{\mathtt{x}}_0 = (x, 0) \in \widehat{M}_0$ and $\overline{m}_\alpha(x)$ as defined by Eq. (8). Then the iterations of the trajectory starting at $\hat{\mathtt{x}}_0$ obey:*

$$S^k_\alpha(x,0) = \begin{cases} (x,k) & \text{for} \quad 0 \quad \le k < \overline{m}_\alpha(x)\,, \\ (x, \widetilde{m}_{\alpha,k}(x)) & \text{for} \quad \overline{m}_\alpha(x) \le k\,, \end{cases} \tag{10a}$$

where

$$\widetilde{m}_{\alpha,k}(x) = \begin{cases} \overline{m}_\alpha(x) & \text{for} \quad (k - \overline{m}_\alpha(x)) \ \textit{is even}\,, \\ \overline{m}_\alpha(x) - 1 & \text{for} \quad (k - \overline{m}_\alpha(x)) \ \textit{is odd}\,. \end{cases} \tag{10b}$$

Proof. This is a consequence of Lemma 1 and Eq. (4). As long as $k < \overline{m}_\alpha(x)$, the forthcoming iteration with S_α increases the cell index by one. For $k \ge \overline{m}_\alpha(x)$ the trajectory alternates between the cells $\overline{m}_\alpha(x)$ and $\overline{m}_\alpha(x) - 1$. □

Remark 3 *Lemma 1 and Proposition 2 imply that every trajectory starting at $\hat{\mathtt{x}}$ with $\pi_{[0,1]}(\hat{\mathtt{x}}) \in [1/2, 1)$ is ballistic for a finite time, and then it gets localised eventually, turning periodic of period 2.*

Remark 4 *The trajectories starting at $\hat{\mathtt{x}}$ with $\pi_{[0,1]}(\hat{\mathtt{x}}) = 1/2$ or $\pi_{[0,1]}(\hat{\mathtt{x}}) = 1$ do not satisfy Eq. (7). Hence, they are forever ballistic, but they constitute a set of zero measure.*

To investigate the transport properties of the SM, we observe that the function

$$\overline{m}_\alpha(x) : (1/2,\ 1) \to \mathbb{N} \tag{11}$$

is a step function with unitary jumps at the points $\ell^+_m(\alpha)$, such that

$$x \in (\ell^+_{k-1}(\alpha), \ell^+_k(\alpha)] \mapsto \overline{m}_\alpha(x) = k\,. \tag{12}$$

Then, the following properties are satisfied:

1. $\overline{m}_\alpha(x)$ is not decreasing: $x_1 < x_2$ implies $\overline{m}_\alpha(x_1) \le \overline{m}_\alpha(x_2)$,
2. $\overline{m}_\alpha(x)$ is left continuous: $\lim_{h\to 0^-} \overline{m}_\alpha(\ell^+_k(\alpha) + h) = \overline{m}_\alpha(\ell^+_k(\alpha)) = k$,
3. $\lim_{x\to 1/2^+} \overline{m}_\alpha(x) = 1,\ \lim_{x\to 1^-} \overline{m}_\alpha(x) = \infty$,
4. $\alpha_1 < \alpha_2$ implies $\overline{m}_{\alpha_1}(x) \ge \overline{m}_{\alpha_2}(x)$, since $\ell^+_j(\alpha_1) > \ell^+_j(\alpha_2)$ for $j > 0$.

The points belonging to a strip $(\ell^+_{k-1}(\alpha), \ell^+_k(\alpha)] = \overline{m}_\alpha{}^{-1}(k)$ share the same fate. Hence, the transport properties of the SM depend on the rate at which such strips shrink with growing k.

Indeed, an ensemble of initial conditions $\widehat{E}_0$, *i.e.* a set of points contained in $(1/2, x_0) \times \{0\} \subset \widehat{M}_0$ with $x_0 < 1$, represents a coarse-grained version of the Dirac δ initial distribution, as commonly considered in diffusion theory. This ensemble reaches localisation: the set $\{\pi_{\mathbb{Z}}(S^j_\alpha(\widehat{E}_0)), j \in \mathbb{N}_0\}$ is bounded. After all, the travelled distance does not exceed $\overline{m}_\alpha(x_0)$, which is finite. Consequently, non-trivial transport properties *necessarily* require the initial ensemble $\widehat{E}_0$ to obey the condition:

$$\sup_{x \in \pi_{[0,1]}(\widehat{E}_0)} \overline{m}_\alpha(x) = \infty, \tag{13a}$$

or, equivalently, to accumulate at $x = 1$:

$$\sup(\pi_{[0,1]}(\widehat{E}_0)) = 1\,, \tag{13b}$$

however, note that condition (13a) (or (13b)) is not sufficient for non trivial behaviour, see Remark 7. Then in order to study transport, we take an ensemble of *uniformly distributed* initial conditions $\widehat{E}_0 \subset (1/2, 1) \times \{0\}$ —analogous to the setting in Burioni et al. (2010)—and characterise the transport properties of the SM by computing the corresponding ensemble averages. Then, $\overline{m}_\alpha(x)$ is the distance travelled by the point $\hat{\mathbf{x}} \in \widehat{E}_0$, with $\pi_{[0,1]}(\hat{\mathbf{x}}) = x$. Consequently, the *mean maximum displacement* and the *mean maximum square displacement* are given by

$$\langle \max_n \Delta\hat{\mathbf{x}}_n \rangle = \frac{1}{\lambda(\pi_{[0,1]}(\widehat{E}_0))} \int\limits_{\pi_{[0,1]}(\widehat{E}_0)} \overline{m}_\alpha(x)\, dx, \text{ and } \langle \max_n \Delta\hat{\mathbf{x}}_n^2 \rangle = \frac{1}{\lambda(\pi_{[0,1]}(\widehat{E}_0))} \int\limits_{\pi_{[0,1]}(\widehat{E}_0)} \overline{m}_\alpha^2(x)\, dx\,, \tag{14}$$

respectively, where $\lambda(\pi_{[0,1]}(\widehat{E}_0)) \leq 1/2$ is the Lebesgue measure of the projection of $\widehat{E}_0$ on $[0, 1]$. Here and in the following, we denote by $\langle\cdot\rangle$ the ensemble average, *i.e.* the average with respect to the Lebesgue measure normalized on $\pi_{[0,1]}(\widehat{E}_0)$, and we assume that $\widehat{E}_0 = (1/2, 1) \times \{0\}$.

These averages do not depend on time. However, they indicate what can be expected for the time evolution of the average travelled distance and mean-square distance. To understand this point, we observe that in each interval $(\ell^+_{k-1}(\alpha), \ell^+_k(\alpha)]$, $k \in \mathbb{N}$ the function $\overline{m}_\alpha(x)$ takes the constant value k. We denote the length of these intervals by:

$$\Delta_k(\alpha) := \ell^+_k(\alpha) - \ell^+_{k-1}(\alpha)\,. \tag{15a}$$

By construction their length adds up to 1/2,

$$\sum_{k=1}^{\infty} \Delta_k(\alpha) = \frac{1}{2}, \tag{15b}$$

and to leading order in k, we have:

$$\Delta_k(\alpha) = \frac{\alpha}{k^{\alpha+1}} \left(1 - \frac{\tilde{c}(\alpha)}{k} + O(k^{-2})\right) \qquad \text{with} \quad \tilde{c}(\alpha) = (1+\alpha)\left(2^{1/\alpha} - \frac{1}{2}\right). \tag{15c}$$

Then, recalling that $\widehat{E}_0 = (1/2, 1) \times \{0\}$, one finds

$$\langle \Delta\hat{\mathbf{x}} \rangle = 2 \int\limits_{1/2}^{1} \overline{m}_\alpha(x)\, dx = 2 \sum_{k=1}^{\infty} k\, \Delta_k(\alpha) = 2 \sum_{k=1}^{\infty} \frac{\alpha}{k^\alpha} \left(1 + O(k^{-1})\right), \tag{16a}$$

where Eqs. (12) and (15c) have been used. Thus, $\langle \Delta\hat{\mathbf{x}} \rangle$ converges for $\alpha > 1$, and it diverges otherwise. Analogously, the mean maximum square displacement is

$$\langle \Delta\hat{\mathbf{x}}^2 \rangle = 2 \int\limits_{1/2}^{1} \overline{m}_\alpha^2(x)\, dx = 2 \sum_{k=1}^{\infty} k^2 \Delta_k(\alpha) = 2 \sum_{k=1}^{\infty} \frac{\alpha}{k^{\alpha-1}} \left(1 + O(k^{-1})\right). \tag{16b}$$

For $\alpha > 2$ the square displacement, $\langle \Delta\hat{\mathbf{x}}^2 \rangle$, is finite. This corresponds to the localisation phenomenon described in Remark 6 of Salari et al. (2015). It arises from the fact that $\ell^+_k(\alpha)$ tends to 1 faster, and transport of the SM is slower, for larger α. On the other hand, for $0 < \alpha < 2$ the mean maximum square displacement diverges, and it is of interest to explore the rate at which this divergence takes place, *i.e.* to determine the *transport exponent* γ.

2.2 Time Evolution of the Displacement Moments

Each particle moves by exactly one step in each time step. Hence, trajectories reach at most site n in n time steps, and the distance $\Delta\hat{\mathrm{x}}_n$ travelled by $\hat{\mathbf{x}} = (x, 0)$ at time n is given by

$$\min\{\widetilde{m}_{\alpha,n}(x), n\}\,, \tag{17}$$

cf. Eq. (10). Moreover, for even and odd times n the displacement $\Delta\hat{\mathrm{x}}_n$ also takes even and odd values, respectively. The corresponding (time-dependent) mean-square displacement can be written as

$$\begin{aligned}\langle\Delta\hat{\mathrm{x}}_n^2\rangle &= 2\int_{1/2}^{1}\min\{\widetilde{m}_{\alpha,n}(x), n\}^2\,dx \\ &= \begin{cases} 2\sum_{i=1}^{(n/2)-1}(2i)^2\left(\Delta_{2i}(\alpha)+\Delta_{2i+1}(\alpha)\right)+2n^2\sum_{k=n}^{\infty}\Delta_k(\alpha) & \text{for}\quad \text{n even}\,, \\ 2\sum_{i=1}^{(n-1)/2}(2i-1)^2\left(\Delta_{2i-1}(\alpha)+\Delta_{2i}(\alpha)\right)+2n^2\sum_{k=n}^{\infty}\Delta_k(\alpha) & \text{for}\quad \text{n odd}\,. \end{cases}\end{aligned} \tag{18a}$$

The sums involving terms $k \geq n$ collect the particles that make n steps to the right and never turned back. Salari et al. (2015) denoted this as the travelling area. It is the same in both cases. The other sum accounts for particles that turn back at least once. Consequently, the particles get localised within n time steps. This represents the term called sub-travelling area in Salari et al. (2015). To leading order this contribution to the mean-square displacement takes the same for odd and even n. Hence, we write:

$$\langle\Delta\hat{\mathrm{x}}_n^2\rangle = 2\int_{1/2}^{1}\min\{\widetilde{m}_{\alpha,n}(x), n\}^2\,dx = 2\sum_{k=1}^{n-1}k^2\Delta_k(\alpha)\,\left(1+O(k^{-1})\right)+2n^2\sum_{k=n}^{\infty}\Delta_k(\alpha)\,. \tag{18b}$$

The asymptotic behaviour of the first sum is:[3]

$$2\sum_{k=1}^{n-1}k^2\Delta_k(\alpha) = 2\sum_{k=1}^{n-1}\frac{\alpha}{k^{\alpha-1}}\,\left(1+O(k^{-1})\right) \sim \begin{cases} \frac{2\,\alpha}{2-\alpha}n^{2-\alpha} & \text{for}\quad 0<\alpha<2\,, \\ 4\,\ln n & \text{for}\quad \alpha=2\,, \\ \text{const} & \text{for}\quad \alpha>2\,. \end{cases} \tag{19a}$$

The form of this scaling can be guessed by interpreting the sum as a Riemann-sum approximation of the integral $\int_1^n x^{1-\alpha}\,dx$. A formal derivation is given in Appendix A. The second sum can be evaluated based on the definition of $\Delta_k(\alpha)$,

$$2\,n^2\sum_{k=n}^{\infty}\Delta_k(\alpha) = 2\,n^2\,\ell_{n-1}(\alpha) = 2\,n^2\,n^{-\alpha}\left(1-\frac{\alpha\,2^{1/\alpha}}{n}+O(n^{-2})\right) \sim 2\,n^{2-\alpha}\,. \tag{19b}$$

Remark 5 *According to Eqs.* (19a) *and* (19b) *the travelling and the sub-travelling areas have the same asymptotic scaling.*

Altogether, we find that the mean-square displacement scales like

$$\langle\Delta\hat{\mathrm{x}}_n^2\rangle \sim \begin{cases} \frac{4}{2-\alpha}\,n^{2-\alpha} & \text{for}\quad 0<\alpha<2\,, \\ 4\,\ln n & \text{for}\quad \alpha=2\,, \\ \text{const} & \text{for}\quad \alpha>2\,. \end{cases} \tag{20}$$

[3] By $f_1(n) \sim f_2(n)$ we mean $f_1(n)/f_2(n) \to 1$ as $n \to \infty$.

The computation of other moments $\langle|\Delta\hat{\mathrm{x}}_n|^p\rangle$, with $p > \alpha$, can be obtained in the same way, based on the same integral representation:

$$\begin{aligned}\langle|\Delta\hat{\mathrm{x}}_n|^p\rangle &= 2\int_{1/2}^{1}\min\{\widetilde{m}_{\alpha,n}(x),n\}^p\,dx \;\sim\; 2\sum_{k=1}^{n-1}k^p\Delta_k(\alpha)\left(1+O(k^{-1})\right)+2n^p\sum_{k=n}^{\infty}\Delta_k(\alpha)\\ &\sim \begin{cases}\frac{2\,p}{p-\alpha}\,n^{p-\alpha} & \text{for}\quad 0<\alpha<p\,,\\ 2\,p\,\ln n & \text{for}\quad \alpha=p\,,\\ \text{const} & \text{for}\quad \alpha>p\,,\end{cases}\end{aligned} \tag{21}$$

because

$$\sum_{k=1}^{n-1}k^p\Delta_k(\alpha)=2\sum_{k=1}^{n-1}\frac{\alpha}{k^{\alpha-p+1}}\left(1+O(k^{-1})\right)\sim\begin{cases}\frac{2\,\alpha}{p-\alpha}\,n^{p-\alpha} & \text{for}\quad 0<\alpha<p\,,\\ 2\,p\,\ln n & \text{for}\quad \alpha=p\,,\\ \text{const} & \text{for}\quad \alpha>p\,.\end{cases} \tag{22}$$

We hence reproduced central results of Salari et al. (2015) in a formalism that is suitable to compute the position-position auto-correlation function. These findings are summarised by the following theorem.

Theorem 6: *Given $0 \le \alpha < 2$, the transport exponent of the Slicer Dynamics with uniformly distributed initial condition in $\widehat{M}_0$ takes the value $\gamma = 2-\alpha$, and the behaviour is*

1. *ballistic if $\alpha = 0$,*
2. *super-diffusive if $0 < \alpha < 1$,*
3. *diffusive if $\alpha = 1$,*
4. *sub-diffusive if $1 < \alpha < 2$,*
5. *logarithmically growing for the mean-square displacement, $\langle\Delta\hat{\mathrm{x}}_n^2\rangle \sim \ln n$, if $\alpha = 2$.*

For $\alpha > 2$ the dynamics has

6. *bounded mean-square displacement $\langle\Delta\hat{\mathrm{x}}_n^2\rangle$.*

Furthermore, for $p > \alpha$ the moments satisfy $\langle|\Delta\hat{\mathrm{x}}_n|^p\rangle \sim n^{p-\alpha}$.

Remark 7: *The parameter dependence of the transport exponent γ depends on the initial distribution.*

For instance, suppose that the x-component of the initial conditions has got density ρ with respect to the uniform measure dx in the interval $(1/2, 1)$. Then, in place of Eq. (18) we have

$$\langle\Delta\hat{\mathrm{x}}_n^2\rangle_\rho = 2\int_{1/2}^{1}\min\{\widetilde{m}_{\alpha,n}(x),n\}^2\,\rho(x)\,dx\,. \tag{23}$$

If the support of ρ does not contain a (left) neighbourhood of 1, then $\langle\Delta\hat{\mathrm{x}}_n^2\rangle \to \text{const}$ as $n\to\infty$ even for $\alpha < 1$. Hence, different asymptotic behaviours arise from different distributions supported in a neighbourhood of 1. For instance, take $\rho(x) = O((1-x)^r)$ as $x \to 1^-$ with $r > -1$. Then, different values of r produce different kinds of diffusion, even at fixed α. Specifically, for the ensemble

$$\rho(x)=\begin{cases}r\,2^{r-1}\,\left(\frac{1}{2}-x\right)^{r-1} & \text{for}\quad 0\le x\le\frac{1}{2}\,,\\ r\,2^{r-1}\,(1-x)^{r-1} & \text{for}\quad \frac{1}{2}<x\le 1\,,\end{cases} \tag{24}$$

one finds that

$$\langle \Delta\hat{\mathrm{x}}_n^2 \rangle_\rho \sim \begin{cases} \frac{2^{r+1}}{2-r\alpha}\, n^{2-r\alpha} & \text{for} \quad 0 < r\,\alpha < 2\,, \\ 2^{r+1}\,\ln n & \text{for} \quad r\,\alpha = 2\,, \\ \text{const} & \text{for} \quad r\,\alpha > 2\,. \end{cases} \tag{25}$$

The transport exponent $\gamma = 2 - r\,\alpha$ depends continuously on r, and only for $r = 1$ (the case of the uniform distribution treated so far) does Eq. (25) reduce to Eq. (20). Different initial distributions lead the SM to different transport properties, as already observed in other frameworks, such as those of Lévy walks (Burioni et al., 2010). However, the dynamical mechanisms underlying this finding are drastically different.

Remark 8: *The anomalous behaviour of the SM with $\alpha \neq 1$ coincides with the persistence of memory. This is in accordance with the common observation in thermodynamic systems that slow decay of correlation leads to anomalous transport, while rapid decay of correlations leads to normal diffusion. However, for $\alpha = 1$ the statistics of the SM appear still like normal diffusion, although memory persists in this case, just as it does for $\alpha \neq 1$. Hence, the SM illustrates that a statistical coincidence in certain phenomena should not be taken as a thermodynamic phenomenon when no thermodynamics is present (see Rondoni and Cohen, 2000, for another example).*

In the case of the SM, the term *transport* must then be used with a grain of salt.

In the following, we explore whether correlations might help to distinguish the SM from the LLg. To this end we analytically compute various scaling limits of the position-position auto-correlations generated by the SM, and compare them with numerically computed correlations of the LLg with the same exponent γ.

2.3 Position-Position Correlations in the Slicer Dynamics

Let us introduce the position-position auto-correlation function as:

$$\phi(n,m) \;:=\; \langle \pi_{\mathbb{Z}}(S^n(\hat{\mathrm{x}}))\; \pi_{\mathbb{Z}}(S^m(\hat{\mathrm{x}}))\rangle := \langle \Delta\hat{\mathrm{x}}_n\, \Delta\hat{\mathrm{x}}_m\rangle \tag{26a}$$

$$= \; 2\int_{1/2}^{1} \min\{\widetilde{m}_{\alpha,m}(x), m\}\, \min\{\widetilde{m}_{\alpha,n}(x), n\}\, dx \qquad \text{with } m \leq n\,. \tag{26b}$$

The integration interval $\mathrm{I} := (1/2, 1]$ can be subdivided in three parts, $\mathrm{I} = E_m^< \cup E_{m,n} \cup E_n^>$, defined by

$$\begin{aligned} E_m^< &= \{x \in \mathrm{I} : \widetilde{m}_{\alpha,m}(x) \leq m\} && \Rightarrow\; \min\{\widetilde{m}_{\alpha,m}(x), m\}\, \min\{\widetilde{m}_{\alpha,n}(x), n\} = \widetilde{m}_{\alpha,m}(x)\, \widetilde{m}_{\alpha,n}(x)\,, \\ E_{m,n} &= \{x \in \mathrm{I} : m < \widetilde{m}_{\alpha,n}(x) \leq n\} && \Rightarrow\; \min\{\widetilde{m}_{\alpha,m}(x), m\}\, \min\{\widetilde{m}_{\alpha,n}(x), n\} = m\, \widetilde{m}_{\alpha,n}(x)\,, \\ E_n^> &= \{x \in \mathrm{I} : n < \widetilde{m}_{\alpha,n}(x)\} && \Rightarrow\; \min\{\widetilde{m}_{\alpha,m}(x), m\}\, \min\{\widetilde{m}_{\alpha,n}(x), n\} = m\,n\,. \end{aligned} \tag{27}$$

Then, rewriting the resulting integrals in terms of sums over the intervals where $\overline{m}_\alpha(x)$ takes the constant value k (*cf.* Eq. (18)), one has:

$$\phi(n,m) \;=\; 2\int_{E_m^<} \widetilde{m}_{\alpha,n}(x)\, \widetilde{m}_{\alpha,m}(x)\, dx + 2\,m \int_{E_{m,n}} \widetilde{m}_{\alpha,n}(x)\, dx + 2\,m\,n \int_{E_n^>} dx \tag{28a}$$

$$\sim \; 2\sum_{k=1}^{m} k^2\, \Delta_k(\alpha) + 2\,m \sum_{k=m+1}^{n} k\, \Delta_k(\alpha) + 2\,m\,n \sum_{k=n+1}^{\infty} \Delta_k(\alpha)\,, \quad m \leq n\,. \tag{28b}$$

The first and the third sum have been evaluated in Eqs. (19a) and (19b), respectively. The asymptotic behaviour of the second term depends on the value of α and on the relation between m and n. In the following, we discuss the following examples:

1. $n \to \infty$ with m fixed,

2. $n, m \to \infty$ with fixed $h = n - m$,

3. $n, m \to \infty$ with $n = m + \ell\, m^q$, where ℓ, q are positive constants.

2.3.1 Scaling of $\phi(n,m)$ for $n \to \infty$ with m fixed

In order to evaluate the second sum in Eq. (28b) we observe that

$$2\,m \sum_{k=m+1}^{n} k\,\Delta_k(\alpha) \quad = \quad 2\,m \sum_{k=0}^{n} k\,\Delta_k(\alpha) - 2\,m \sum_{k=0}^{m} k\,\Delta_k(\alpha)\,. \tag{29}$$

For fixed m, the latter sum takes a constant value, and for $n \to \infty$ the former sum scales as (*cf.* Eq. (22) or the formal derivation provided in Appendix A)

$$2\,m \sum_{k=0}^{n} k\,\Delta_k(\alpha) \sim \begin{cases} \frac{2\,\alpha\,m}{1-\alpha}\, n^{1-\alpha} & \text{for} \quad 0 < \alpha < 1\,, \\ 2\,m\,\ln n & \text{for} \quad \alpha = 1\,, \\ \text{const} & \text{for} \quad \alpha > 1\,. \end{cases} \tag{30}$$

The leading-order scaling of the three sums in Eq. (28b) is summarised in the following lemma:

Lemma 9: *For $n \to \infty$ with fixed m the auto-correlation function, $\phi(n,m)$, defined in Eq.* (26a)*, asymptotically scales as:*

$$\phi(n,m) \sim \begin{cases} \frac{2\,m}{1-\alpha}\, n^{1-\alpha} & \textit{for} \quad 0 < \alpha < 1\,, \\ 2\,m\,\ln n & \textit{for} \quad \alpha = 1\,, \\ \textit{const} & \textit{for} \quad \alpha > 1\,. \end{cases} \tag{31}$$

Proof. The first sum in (28b) has a finite number of terms that all take finite positive values. Hence, it adds to a finite positive number. For $0 < \alpha < 1$ the leading-order contributions of the second and the third sum have the same scaling, $n^{1-\alpha}$, which diverges for $n \to \infty$. From Eqs. (30) and (19b) we have

$$\phi(n,m) \sim 2\,m\,\left(\frac{\alpha}{1-\alpha} + 1\right)\, n^{1-\alpha} = \frac{2\,m}{1-\alpha}\, n^{1-\alpha} \qquad \text{for } 0 < \alpha < 1\,.$$

For $\alpha = 1$ the exponent $1 - \alpha = 0$ such that the third term also takes a finite value. In that case the leading-order scaling is provided by the second sum, Eq. (30).

Finally, for $\alpha > 1$ all sums contributing to Eq. (26a) take constant values. □

The dashed lines in Figure 1a show the asymptotic behaviour, Eq. (31), for $\alpha = 1/2$ and different fixed values of m. They provide an excellent description of the asymptotic behaviour of the numerical evaluation of the definition, Eq. (26a) (solid lines). The lower panel of the figure demonstrates that the ratio of the correlation function and the prediction of its asymptotic behaviour approaches one for a vast range of different values of m.

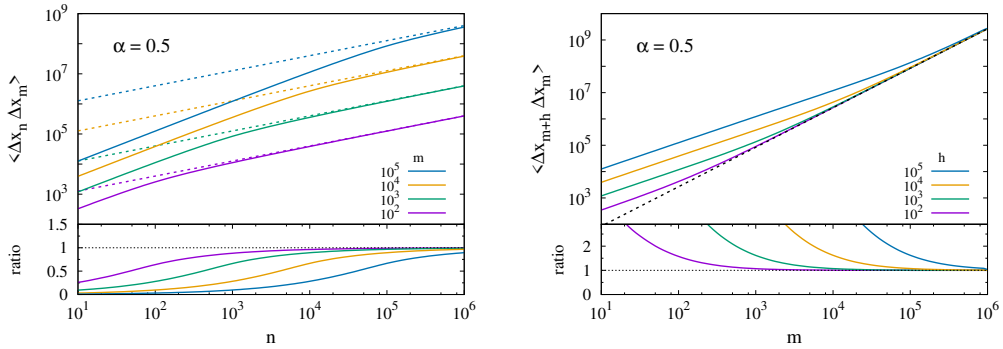

(a) Correlations for fixed time m. (b) Correlations for fixed time lag $h = n - m$.

Figure 1: Comparison of the auto-correlation function, $\phi(n, m)$, and expressions for its asymptotic scaling, for $\alpha = 1/2$ in two different cases. The functions $\phi(n, m)$ obtained from the sums of Eq. (28b) are plotted as solid lines. The respective asymptotic expressions are indicated by dashed lines. (a) The limit of large n for a for fixed value of m. The values of m are provided in the figure legend in the order of the lines from top to bottom. The asymptotic scaling is provided by Eq. (31). (b) The large-m limit for a fixed time lag $h = n - m$. The values of h are provided in the figure legend in the order of the lines from top to bottom. The asymptotic scaling is provided by Eq. (33). In the lower panels we show the ratio of the auto-correlation function and the respective asymptotic expressions.

2.3.2 Scaling of $\phi(m + h, m)$ for $m \to \infty$ with $h > 0$ fixed

In this case, the second sum in Eq. (28b) involves a finite number of positive terms. The sum can be bounded from above by

$$2\,m \sum_{k=m+1}^{m+h} k\,\Delta_k(\alpha) = 2\,\alpha\,m \sum_{k=m+1}^{m+h} k^{-\alpha} \left(1 - \frac{\tilde{c}(\alpha)}{k} + O(k^{-2})\right)$$

$$< 2\,\alpha\,h\,m^{1-\alpha} \left(1 - \frac{\tilde{c}(\alpha)}{m+h} + O(m^{-2})\right) < \begin{cases} 2\,\alpha\,h\,(m+h)^{1-\alpha} & \text{for} \quad 0 < \alpha < 1\,, \\ 2\,\alpha\,h & \text{for} \quad 1 \le \alpha\,. \end{cases}$$

and from below by

$$2\,m \sum_{k=m+1}^{m+h} k\,\Delta_k(\alpha) > 2\,\alpha\,h\,m\,(m+h)^{-\alpha}\,\left(1 + O(m^{-1})\right) > \begin{cases} 2\,\alpha\,h\,m^{1-\alpha} & \text{for} \quad 0 < \alpha < 1\,, \\ 0 & \text{for} \quad 1 \le \alpha\,. \end{cases}$$

Noting that constant h implies $(m+h)^{1-\alpha} = m^{1-\alpha}\,(1 + h/m)^{1-\alpha} \sim m^{1-\alpha}$ we find that the second sum scales as

$$2\,m \sum_{k=m+1}^{m+h} k\,\Delta_k(\alpha) \sim \begin{cases} 2\,\alpha\,h\,m^{1-\alpha} & \text{for} \quad 0 < \alpha < 1\,, \\ O(1) & \text{for} \quad 1 \le \alpha\,. \end{cases} \tag{32}$$

Hence, the leading-order scaling of the auto-correlation function takes the form:

Lemma 10: *For $m \to \infty$ with fixed $n - m = h = const$ the auto-correlation function, $\phi(m + h, m)$, asymptotically scales as:*

$$\phi(m+h, m) \sim \begin{cases} \frac{4}{2-\alpha}\,m^{2-\alpha} & \textit{for} \quad 0 < \alpha < 2\,, \\ 4\,\ln(m) & \textit{for} \quad \alpha = 2\,, \\ \textit{const} & \textit{for} \quad \alpha > 2\,. \end{cases} \tag{33}$$

Proof. For $0 < \alpha < 2$ the leading-order contributions of the first and third term in Eq. (28b) have the same scaling, $m^{2-\alpha}$. These terms dominate the scaling of the second sum, Eq. (32). In this range one hence recovers the scaling of the mean-square displacement in Eq. (20).

For $\alpha = 2$ the second and third terms in Eq. (28b) take constant values, while the first one diverges logarithmically according to Eq. (19a).

Finally, for $\alpha > 2$ all sums contributing to Eq. (28b) take constant values. □

The dashed lines in Figure 1b show the asymptotic behaviour, Eq. (33), for $\alpha = 1/2$, and different time lags $h = n - m$. They provide an excellent description of the asymptotics of the numerical evaluation of the definition, Eq. (26a) (solid lines). The lower panel of the figure demonstrates that the ratio of the auto-correlation function and the prediction of its asymptotic behaviour approaches 1 for a vast range of values of h.

The correlation function $\phi(m+h, m)$ looks like correlation functions addressing the time-translation invariance of the position-position auto-correlation function $\phi(t_1, t_2)$ for fixed time increments $t_2 - t_1 = h$. However, this impression is misleading: here, we consider an ensemble where all members start close to the origin. Therefore, the behaviour of the correlations for large m characterizes the decay of features of the initial ensemble rather than referring to translations in time. In order to clearly make this point we consider the large m scaling of $\phi(m + \ell m^q, m)$. For $q < 1$ the difference of the two times will become negligible as compared to the mean. For $q > 1$ the difference between t_1 and t_2 grows.

2.3.3 Scaling of $\phi(m + \ell m^q, m)$ for $m \to \infty$ with $\ell > 0$

For $q < 1$, $q = 1$, and $q > 1$ the auto-correlation function shows different scalings.

Scaling for $q < 1$. In this case bounds for the second sum in Eq. (28b) can be provided by a calculation fully analogous to the derivation of Eq. (32). This provides the scaling

$$2\,m \sum_{k=m+1}^{m+h} k\,\Delta_k(\alpha) \sim \begin{cases} 2\,\alpha\,\ell\,m^{1-q-\alpha} & \text{for} \quad 0 < \alpha < 1\,, \\ O(1) & \text{for} \quad 1 \le \alpha\,. \end{cases}$$

This scaling is always sub-dominant with respect to those of the other two sums in Eq. (28b). As far as the asymptotic scaling is concerned we have the same situation as for fixed $n - m = h$, and the auto-correlation function has the same scaling in these two limits.

Lemma 11: *For $q < 1$, $\ell > 0$, and $m \to \infty$ the auto-correlation function, $\phi(m + \ell m^q, m)$ follows the same asymptotic scaling, Eq.* (33)*, as for the case where the time difference between the arguments is constant,*

$$\phi(m + \ell\,m^q, m) \sim \phi(m + h, m) \qquad \textit{for} \quad \ell, h > 0 \quad \textit{and} \quad q < 1\,. \tag{34}$$

Scaling for $q = 1$. In this case we have $n = m + \ell\,m^q = (1 + \ell)m$, *i.e.* n is proportional to m. In order to find the scaling for large m, we start from Eq. (29). For $\alpha \neq 1$ the two sums on the right-hand side scale like a power law with exponent $1 - \alpha$ and a constant offset that is relevant when $\alpha > 1$. The constant drops out when taking the difference, so that we obtain

$$2\,m \sum_{k=m+1}^{n} k\,\Delta_k(\alpha) \quad \sim \quad \frac{2\,m\,\alpha}{1-\alpha}\,\left(n^{1-\alpha} - m^{1-\alpha}\right) \tag{35a}$$

$$= \quad \frac{2\,\alpha}{1-\alpha}\,\left((\ell+1)^{1-\alpha} - 1\right)\,m^{2-\alpha} \qquad \text{for} \quad \alpha \neq 1\,. \tag{35b}$$

Moreover, for $\alpha = 1$ the sum diverges logarithmically:

$$2\,m \sum_{k=m+1}^{n} k\,\Delta_k(\alpha) \sim 2\,m\,\alpha\,\ln\frac{n}{m} = 2\,m\,\ln(1+\ell) \qquad \text{for} \quad \alpha = 1\,. \tag{35c}$$

Hence, the leading-order scaling of the auto-correlation function is given by:

Lemma 12: *For any $\ell > 0$ the auto-correlation function, $\phi((1+\ell)\,m, m)$, asymptotically scales as:*

$$\phi((1+\ell)\,m, m) \sim \begin{cases} \frac{2}{1-\alpha}\left((1+\ell)^{1-\alpha} - \frac{\alpha}{2-\alpha}\right)\,m^{2-\alpha} & \textit{for} \quad 0<\alpha<2, \quad \alpha\neq 1\,, \\ (4+2\,\ln(1+\ell))\;m & \textit{for} \quad \alpha = 1\,, \\ 4\,\ln(m) & \textit{for} \quad \alpha = 2\,, \\ \textit{const} & \textit{for} \quad \alpha > 2\,. \end{cases} \tag{36}$$

Proof. The cases $\alpha \geq 2$ are obtained as in Lemma 9.

For $0 < \alpha < 2$ the leading-order contributions to all three sums in Eq. (28a) scale like $m^{2-\alpha}$. The case $\alpha = 1$ is special, however, because the second sum takes a different prefactor, Eq. (35c), rather the one obtained in Eq. (35b). For $0 < \alpha < 2$ and $\alpha \neq 1$ we have

$$\phi((1+\ell)\,m, m) \sim \left(\frac{2\,\alpha}{2-\alpha} + \frac{2\,\alpha}{1-\alpha}\;\left((1+\ell)^{1-\alpha} - 1\right) + 2\,(1+\ell)^{1-\alpha}\right)\;m^{2-\alpha}\,,$$

while for $\alpha = 1$ we have

$$\phi((1+\ell)\,m, m) \sim (2 + 2\;\ln(1+\ell) + 2)\;m\,.$$

The result indicated in Eq. (36) is obtained after collecting terms. □

Scaling for $q > 1$. In this case Eq. (35a) still applies, but $n^{1-\alpha}$ is the dominating term in the bracket for $\alpha > 1$, while $m^{1-\alpha}$ is the dominating term in the bracket for $\alpha < 1$. Moreover, the logarithm in the scaling provided in Eq. (35c) now scales as $\ln(n/m) = \ln(1+\ell\,m^{q-1}) \sim (q-1)\,\ln(m)$. When we further observe that $n \sim \ell\,m^q$, this implies

$$2\,m \sum_{k=m+1}^{n} k\,\Delta_k(\alpha) \quad \sim \quad \begin{cases} \frac{2\,\ell\,\alpha}{1-\alpha}\,m^{1+q\,(1-\alpha)} & \text{for} \quad 0<\alpha<1\,, \\ 2\,(q-1)\,m\,\ln(m) & \text{for} \quad \alpha = 1\,, \\ \frac{2\,\alpha}{\alpha-1}\,m^{2-\alpha} & \text{for} \quad \alpha > 1\,. \end{cases} \tag{37}$$

Hence, the leading-order scaling of the auto-correlation function obeys the following:

Lemma 13: *For $q > 1$, $\ell > 0$, and $m \to \infty$ the auto-correlation function, $\phi(m + \ell\,m^q, m)$ asymptotically scales as:*

$$\phi(m+\ell\,m^q, m) \sim \begin{cases} \frac{2}{1-\alpha}\,\ell^{1-\alpha}\,m^{1+q\,(1-\alpha)} & \textit{for} \quad 0<\alpha<1\,, \\ 2\,(q-1)\,m\,\ln(m) & \textit{for} \quad \alpha = 1\,, \\ \frac{2\,\alpha}{(2-\alpha)\,(\alpha-1)}\,m^{2-\alpha} & \textit{for} \quad 1<\alpha<2\,, \\ 4\,\ln(m) & \textit{for} \quad \alpha = 2\,, \\ \textit{const} & \textit{for} \quad \alpha > 2\,. \end{cases} \tag{38}$$

Proof. The cases $\alpha \geq 2$ are obtained as in Lemma 9.

For $1 < \alpha < 2$ the leading-order contributions scale like $m^{2-\alpha}$. They appear in the first and in the second sum on the right-hand-side of Eq. (28b). Collecting the corresponding terms in Eqs. (19a) and (37) we obtain

$$\phi(m + \ell\, m^q, m) \sim \left(\frac{2\,\alpha}{2-\alpha} + \frac{2\,\alpha}{\alpha - 1} \right) m^{2-\alpha} = \frac{2\,\alpha}{(2-\alpha)\,(\alpha-1)}\, m^{2-\alpha}\,.$$

For $\alpha = 1$ the leading-order scaling contribution to the auto-correlation function is provided in Eq. (37).

For $0 < \alpha < 1$ the leading-order contributions scale like $m\, n^{1-\alpha} \sim \ell^{1-\alpha}\, m^{1+q\,(1-\alpha)}$. Collecting these terms in Eqs. (19b) and (37) provides

$$\phi(m + \ell\, m^q, m) \sim \left(\frac{2\,\alpha}{1-\alpha} + 2 \right) \ell^{1-\alpha}\, m^{1+q\,(1-\alpha)} = \frac{2}{1-\alpha}\, \ell^{1-\alpha}\, m^{1+q\,(1-\alpha)}\,.$$

□

3 Comparison of the SM with a Lévy-Lorentz gas

The LLg is a random walk in a one-dimensional random environment (Barkai et al., 2000), where a point particle moves ballistically (with velocity $\pm v$) between static point scatterers. At each scatterer the particle is either transmitted or reflected with probability 1/2. The distance r between two consecutive scatterers is a random variable drawn independently and identically from a Lévy distribution with density:

$$\lambda(r) = \beta r_0^\beta \frac{1}{r^{\beta+1}}, \quad r \in [r_0, +\infty), \tag{39}$$

where $\beta > 0$, and r_0 is the characteristic length scale of the system.

The LLg shares basic similarities with the SM in that both systems deal with non-interacting particles and the initial condition plays an important role. On the other hand, the differences are evident: The LLg is a continuous-time stochastic system, while the slicer dynamics is discrete-time and deterministic. In particular, the LLg dependence on the initial conditions is considerably more intricate than in the SM: the LLg transport properties depend on whether a walker can start its trajectory away from the scatterers, called equilibrium initial condition, or must start exactly at a scatterer, called non-equilibrium initial condition (Barkai et al., 2000; Burioni et al., 2010). The asymptotic behaviour of the moments is known for the LLg with non-equilibrium initial conditions. Hence, we focus on this situation, and we show that for this setting the SM provides insight into transport properties of the LLg.

3.1 Moments of the Displacement

Barkai et al. (2000) calculated bounds for the mean-square displacement for equilibrium and non-equilibrium initial conditions. Subsequently, Burioni et al. (2010) adopted some simplifying assumptions to find the asymptotic form for non-equilibrium conditions of all moments $\langle |r(t)|^p \rangle$ with $p > 0$:

$$\langle |r(t)|^p \rangle \sim \begin{cases} t^{\frac{p}{1+\beta}} & \text{for} \quad \beta < 1,\ p < \beta\,, \\ t^{\frac{p(1+\beta)-\beta^2}{1+\beta}} & \text{for} \quad \beta < 1,\ p > \beta\,, \\ t^{\frac{p}{2}} & \text{for} \quad \beta > 1,\ p < 2\beta - 1\,, \\ t^{\frac{1}{2}+p-\beta} & \text{for} \quad \beta > 1,\ p > 2\beta - 1\,. \end{cases} \tag{40}$$

For the mean-square displacement, $p = 2$, this result implies

$$\langle r(t)^2 \rangle \sim t^\gamma \quad \text{with} \quad \gamma = \begin{cases} 2 - \frac{\beta^2}{(1+\beta)} & \text{for} \quad \beta < 1\,, \\ \frac{5}{2} - \beta & \text{for} \quad 1 \leq \beta < 3/2\,, \\ 1 & \text{for} \quad 3/2 \leq \beta\,. \end{cases} \tag{41}$$

Unlike the SM case, that enjoys sub-diffusive transport for $\alpha > 1$, non-equilibrium initial conditions for the LLg only lead to super-diffusive ($0 < \beta < 3/2$) or diffusive ($\beta \geq 3/2$) regimes: sub-diffusion is not expected.

Salari et al. (2015) observed that the moments of the SM in its super-diffusive regime ($0 < \alpha < 1$) can be mapped to those of the LLg. They proved that all moments of the SM, Eq. (21), scale like those conjectured and numerically validated for the LLg, Eq. (40), once the second moments do. This is the case if the following holds, *cf.* Eqs. (20) and (41):

$$\alpha = \begin{cases} \frac{\beta^2}{(1+\beta)} & \text{for} \quad 0 < \beta \leq 1\,, \\ \beta - \frac{1}{2} & \text{for} \quad 1 < \beta \leq \frac{3}{2}\,, \\ 1 & \text{for} \quad \frac{3}{2} < \beta\,. \end{cases} \tag{42}$$

When adopting this mapping also all other moments of the SM agree with those of the LLg, Eq. (40).

This means that relation Eq. (42) makes the SM and the LLg asymptotically indistinguishable from the viewpoint of moments, provided the assumptions of (Burioni et al., 2010) holds. This equivalence is by no means trivial. In particular, the relation takes different functional forms in different parameters ranges, because the LLg has different scaling regimes for super-diffusive transport, while the SM has only one regime for all kinds of transport. We now explore whether the position-position auto-correlations of the two dynamics differ. The correlations are calculated analytically for the SM. This data will then be compared to numerical data for the LLg. For correlations in the LLg there are no analytic results such as those of (Burioni et al., 2010) for the moments.

3.2 Numerical Implementation of the Lévy-Lorentz Gas

The non-equilibrium initial conditions for the LLg are implemented by starting each particle in the origin $x_0 = 0$, where a scatterer is assumed to be present in all realisations of the scatterers distributed in the line $\mathbb{R}$. Moreover, trajectories that return to the origin provide a minor contribution to the moments for super-diffusive transport. For numerical tests, given the symmetry of the dynamics, we modify the original dynamics of the LLg, placing a reflecting barrier at $x = 0$ and giving an initial positive velocity to each LLg walker. Thus, the resulting system, denoted LLg$^+$, which we numerically verified to yield the same results of the LLg for the position auto-correlation function, evolves in $\mathbb{R}_0^+$, similarly to the SM with initial conditions in $(1/2, 1) \times \{0\}$, that evolve in the half configuration space $\widehat{M}^+$.

More precisely, the setting is as follows. Let $(L_0, L_1, L_2, \ldots)$ be a sequence of i.i.d. random variables with density Eq. (39), and let $Y_{i+1} = Y_i + L_i$, $i = 0, 1, 2, \ldots$, with $Y_0 \equiv 0$. Denote by $\mathtt{Y}$ a given realisation of the sequence $(Y_0 \equiv 0, Y_1, Y_2, \ldots)$, that represents one random scatterers distribution in $\mathbb{R}_0^+$. We introduce the discrete-time process that represents the LLg$^+$at the scattering events. Let $\omega = (\omega_0, \omega_1, \omega_2, \ldots)$ be a random walk on $\mathbb{Z}_0^+$ with the conditions that $\omega_0 \equiv 0$ and $\omega_n - \omega_{n-1}$, $n = 1, 2, \ldots$ are i.i.d. dichotomic variables, known as Rademacher random variables, with $P(\omega_n - \omega_{n-1} = +1 \,|\, \omega_{n-1} \neq 0) = P(\omega_n - \omega_{n-1} = -1 \,|\, \omega_{n-1} \neq 0) = 1/2$, and $P(\omega_n - \omega_{n-1} = +1 \,|\, \omega_{n-1} = 0) = 1$. These conditions mean that the walk starts at 0 and whenever it returns there, it is reflected to the right. Away from 0, each walker follows a simple symmetric random walk. Then, the process that represents the position of the moving particle at the scattering events will be given by $\mathcal{W} = (Y_{\omega_0}, Y_{\omega_1}, Y_{\omega_2}, \ldots)$. From knowledge of $\mathcal{W}$, the continuous-time position $r(t)$ of the corresponding moving particle of the LLg$^+$ can be unambiguously reconstructed, because the velocity between any two scattering events is constant.

The process $r(t)$ is affected by two sources of stochasticity: the environment $\mathtt{Y}$ and the scattering ω. Hence, averages can be taken in two different fashions. Let us denote by $\mathbb{E}_\omega$ the average w.r.t. the process ω, *i.e.* the average over particles that can be identified with their scattering sequences in a given realisation of the environment. Analogously, let $\mathbb{E}_\mathtt{Y}$ denote the average over the random scatterers realisations. Then, the average of $r^2(t)$ at fixed scatterers

configuration $\mathtt{Y}$, is denoted by $\mathbb{E}_\omega(r^2(t)|\mathtt{Y})$. This is a random quantity because $\mathtt{Y}$ is random. Averaging this quantity over the ensemble of scatterers yields the mean-square displacement of the LLg$^+$:

$$\langle r^2(t)\rangle_\beta = \mathbb{E}_\mathtt{Y}[\mathbb{E}_\omega(r^2(t)|\mathtt{Y})]\,. \tag{43}$$

The subscript β indicates that the distribution of scatterers, Eq. (39), depends on β.

This procedure has been implemented in a FORTRAN code by introducing a truncation in the sequence of scattering events $\bar\omega = (\omega_0, \omega_1, \omega_2, \ldots, \omega_N)$ that corresponds to a time $T = T(\bar\omega, \mathtt{Y})$ at which the process $r(t)$ stops. The stopping time $T(\bar\omega, \mathtt{Y})$ is random, and typically large if the scatterers are placed at large distances from one another, *i.e.* for small β. In contrast, for large β, the distances are on average approximately equal r_0.[4] Therefore, one expects typically smaller and smaller $T(\bar\omega, \mathtt{Y})$ for larger and larger β, with the risk of under-sampling the large-time behaviour of the LLg$^+$ in numerical estimates of statistical properties. We do not present data with insufficient statistics.

Our choice of r_0 and v in the numerical simulations of the LLg$^+$ follows Burioni et al. (2010). We set the characteristic length r_0 to 0.1, and the velocity v of the ballistic motion is always 1. The number of simulated scattering events is $N = 2.5 \cdot 10^6$.

We tested the code and explored the relation between the LLg and the LLg$^+$, by calculating the mean-square displacement of the LLg$^+$, in order to verify the power-law behaviour of the LLg, see Eq. (41). Table 1 shows that our numerical results for the mean-square displacement for the LLg$^+$ accurately reproduce the exponent given in Eq. (41) for the LLg, at least for not too large values of β. These results, with similar ones obtained by comparing various position-position auto-correlation functions of the two models, indicate the equivalence of the LLg and the LLg$^+$, at least at the level of the mean-square displacement and some correlation functions. The slightly decreasing accuracy for increasing β, observed in Table 1 and in the computation of correlations, can be attributed to poorer statistics of the numerical estimates, as suggested above. Therefore, in the following we mainly focus on the cases with $\beta \lesssim 1$, while more accurate data for larger β will be presented in forthcoming work.

Finally, we observe that our simulations concern the LLg$^+$ because they are computationally more efficient than simulations of the LLg. This can be heuristically understood by observing that, at a fixed simulation length, the LLg$^+$ dynamics produce trajectories that typically reach larger distances from the origin, than those reached by trajectories of the LLg. This provides better sampling for the long-time behaviour.

3.3 Correlations of the LLg$^+$

For $t, s \geq 0$, we define the position-position auto-correlation function for the LLg$^+$ as follows:

$$\varphi(t,s) = \langle r(t)\, r(s)\rangle_\beta = \mathbb{E}_\mathtt{Y}[\mathbb{E}_\omega(r(t)r(s)|\mathtt{Y})]. \tag{44}$$

We aim at comparing the asymptotic behaviour of $\varphi(t,s)$ with that of the SM auto-correlation function $\phi(n,m)$, Eq. (26a). Following the scaling adopted in Sec. 2.3.1, 2.3.2, and 2.3.3 for the SM we consider three cases:

1. $\varphi(t,s)$ for $t \to \infty$ at a fixed value of s.
2. $\varphi(t+\tau, t)$ for $t \to \infty$ at a fixed value of τ.
3. $\varphi(t + \ell\, t^q, t)$ for $t \to \infty$ at fixed q and $\ell > 0$.

Note that there is no free fit parameter in this comparison of the exponents, when one assumes the relation Eq. (42) between α and β. Here, we verify that α and β obey Eq. (42) when the asymptotic scalings of the position-position auto-correlation functions of the SM and the LLg$^+$ match.

[4] More precisely, if L is distributed according to Eq. (39), then $\mathbb{E}[L] = +\infty$ if $\beta \leq 1$ and $\mathbb{E}[L] = \frac{\beta r_0}{\beta - 1}$ if $\beta > 1$. Moreover the variance is $\frac{\beta\, r_0^2}{(\beta-2)(\beta-1)^2}$ for $\beta > 2$ and $+\infty$ for $\beta \leq 2$. For $\beta \gg 1$ the expected distance is therefore $\mathbb{E}[L] \simeq r_0$ with relative deviations of the order of β^{-1}.

β	γ	
	Eq. (41)	fit to data
0.1	1.99	1.99
0.3	1.93	1.93
0.5	1.83	1.82
0.6	1.77	1.73
0.8	1.64	1.63
1.0	1.50	1.51
1.3	1.20	1.18
2.0	1.00	0.95

Table 1: Comparison of numerical values for the scaling exponent γ of the mean-square displacement in the LLg$^+$ (third column) vs. the prediction of Eq. (41) (second column). The numerical estimate of γ agrees with the expressions for the LLg derived and tested in Burioni et al. (2010).

3.3.1 Correlation $\langle r(t)\, r(s)\rangle_\beta$ with $s > 0$ constant

In Sec. 2.3.1 we provided the scaling of the position-position auto-correlation function for the SM, Eq. (31), when one of its times is fixed. For $0 < \alpha < 1$ we have:

$$\langle \Delta x_n\, \Delta x_m\rangle_\alpha \sim \frac{2\,m}{1-\alpha}\, n^{1-\alpha}, \quad \text{as } n \to \infty. \tag{45}$$

Here and in the following we denote by $\langle\cdot\rangle_\alpha$ the ensemble average of the trajectories of the SM with parameter α. In analogy to the scaling, Eq. (45), we propose the following

Conjecture 14a: *The auto-correlation function of the LLg$^+$ asymptotically scales as the one of the SM. When the time s is fixed, the auto-correlation function $\langle r(t)\, r(s)\rangle_\beta$ obeys:*

$$\lim_{t\to\infty} \frac{\langle r(t)\, r(s)\rangle_\beta}{\frac{2\,s}{w_1}\, t^{w_1}} = C_1 \neq 0\,, \tag{46a}$$

$$\textit{with} \qquad w_1 = 1 - \alpha(\beta) = \gamma(\beta) - 1\,. \tag{46b}$$

Numerical Evidence. The LLg$^+$ correlations $\langle r(t) r(s)\rangle_\beta$ have been computed for several values of s. Numerical results for fixed $s = 2000$ and different values of β between 0.1 and 0.8 are shown in the upper panel of Figure 2a. Moreover, in the upper panel of Figure 2b we show data for $\beta = 0.1$ and six values of s in the range between 500 and 5000.

The respective lower panels show the time dependence of the ratio of Eq. (46a), in order to test its asymptotic convergence. For small β and different s this ratio provides a perfect data collapse (Figure 2b). For larger β the data collapse is still fair in view of the numerical accuracy of our data (Figure 2a). Moreover, the scaling exponents w_1 adopted to achieve the collapse depend on β and they are independent of s. The β-dependence agrees with the values $w_1 = 1 - \alpha(\beta) = \gamma(\beta) - 1$ suggested by the SM (*cf.* the values for $\gamma(\beta)$ provided in Table 1). Consequently, the SM provides a faithful description of the LLg$^+$ auto-correlation function, both as far as the exponents and the the parameter-dependence of the prefactor is concerned. □

3.3.2 Correlation $\langle r(t+\tau)\, r(t)\rangle_\beta$ with $\tau > 0$ constant

In Sec. 2.3.2, we provided the scaling of the auto-correlation function for the SM, Eq. (33)when the difference h between the times is fixed. For $0 < \alpha < 2$ and fixed h, one has

$$\langle \Delta x_{m+h}\, \Delta x_m\rangle_\alpha \sim \frac{4}{2-\alpha} m^{2-\alpha}, \quad \text{as } m \to \infty\,. \tag{47}$$

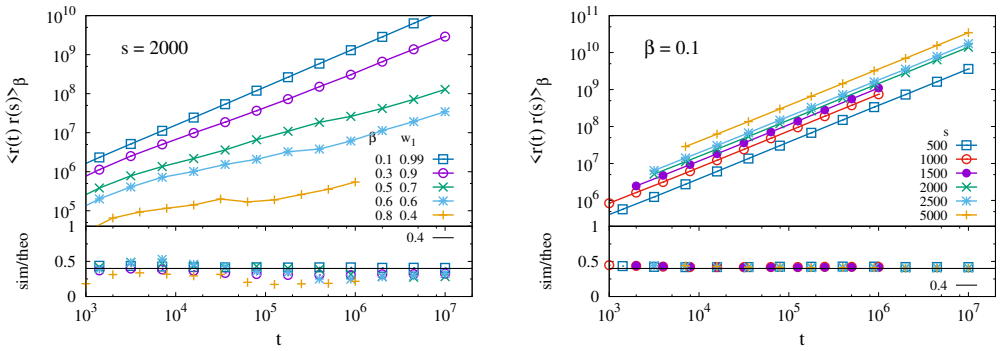

(a) Varying β for fixed $s = 2000$. (b) Varying s for fixed $\beta = 0.1$.

Figure 2: Log-log plots of the correlation $\langle r(t)\, r(s)\rangle_\beta$ as a function of time t, for different values of β and of s. The respective values for β and s are specified in the figure legends. In Figure 2a we also specify the values for the exponents w_1 that provide the best fit to the data. The approach of the data towards the solid line in the bottom panel demonstrates that Eq. (46a) provides a faithful asymptotic scaling, with $C_1 = 0.4$.

In analogy to this scaling we propose the following

Conjecture 14b: *The auto-correlation function of the LLg$^+$ asymptotically scales like the one of the SM. When the time lag h is fixed, the correlation function $\langle r(t)\, r(t+\tau)\rangle_\beta$ obeys:*

$$\lim_{t\to\infty} \frac{\langle r(t+\tau)\, r(t)\rangle_\beta}{\frac{4}{w_2}\, t^{w_2}} = C_2 \neq 0\,, \tag{48a}$$

$$\textit{with} \qquad w_2 = 2 - \alpha(\beta) = \gamma(\beta)\,. \tag{48b}$$

Numerical Evidence. In Figure 3 we show numerical data for (a) a fixed value $\tau = 500$ and β in the range between 0.1 and 0.8, and (b) a fixed value $\beta = 0.1$ and τ in the range between 100 and 8000. The lower panels show the ratio of the numerical data and the theoretical prediction, Eq. (48a). The curves are not globally linear in the log-log plot. However, they approach a power law for sufficiently large values of t, and in that range they nicely follow the asymptotic scaling, Eq. (48a), with $C_2 = 0.45$. The coefficient and the exponent of the asymptotic law are independent of τ and the dependence of w_2 faithfully agrees with the expected value $2 - \alpha(\beta) = \gamma(\beta)$, as provided in Table 1. □

3.3.3 Correlation $\langle r(t + \ell\, t^q)\, r(t)\rangle_\beta$ with $\ell = 1$ and $0 < q < 1$ constant

In Section 2.3.3, we derived the auto-correlation for the SM, Eq. (31). For $0 < q < 1$ and $0 < \alpha < 1$, one has:

$$\langle \Delta x_{m+m^q}\, \Delta x_m\rangle_\alpha \sim \frac{4}{2-\alpha}\, m^{2-\alpha}, \quad \text{as } m \to \infty\,. \tag{49}$$

In analogy to this scaling, we propose the following

Conjecture 14c: *The auto-correlation function of the LLg$^+$ asymptotically scales like the SM. For the time lag ℓt^q with $0 < q < 1$ between its two times, the auto-correlation function*

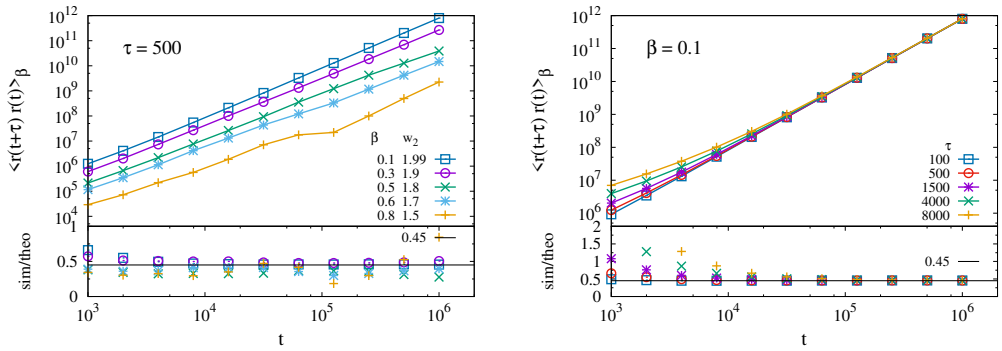

(a) Varying β for fixed $\tau = 500$.

(b) Varying h for fixed $\beta = 0.1$.

Figure 3: Log-log plots of the correlation $\langle r(t+\tau)\, r(t)\rangle_\beta$ as a function of time t for various values of β and of τ. The respective values for β and τ are specified in the figure legends. Figure 3a also specifies the values for the exponents w_2 that provide the best fit to the data. The approach of the data towards the solid line in the bottom panel demonstrates that Eq. (48a) provides a faithful asymptotic scaling, with $C_2 = 0.45$.

$\langle r(t)\, r(t+\ell\, t^q)\rangle_\beta$ *obeys:*

$$\lim_{t\to\infty} \frac{\langle r(t+\ell\, t^q)\, r(t)\rangle_\beta}{\frac{4}{w_3}\, t^{w_3}} = C_3 \neq 0\,, \tag{50a}$$

$$\textit{with} \qquad w_3 = 2 - \alpha(\beta) = \gamma(\beta)\,. \tag{50b}$$

Numerical Evidence. In Figure 4, we show numerical data for (a) a fixed value $q = 0.7$ and β in the range between 0.1 and 0.8, and (b) a fixed value $\beta = 0.1$ and q in the range between 0.1 and 0.9. The lower panels show the ratio of the numerical data and expected scaling, Eq. (50a). Also in this case there is an excellent agreement between the data and the proposed asymptotic scaling. □

4 Discussion

The investigation of the relation between the SM and the LLg started in Salari et al. (2015) with the demonstration of the equivalence of the scalings of the time-dependent moments of the displacement. Because it is well known that moments do not sufficiently characterise transport processes (Sokolov, 2012), we have extended that study here to position-position auto-correlation functions. We analytically computed the position-position auto-correlation function $\phi(n, m)$ of the SM, and we derived the asymptotic behaviour of this function in several cases corresponding to different relations between the times m and n. Then, we numerically estimated the position-position auto-correlation function of the LLg$^+$, in order to estimate its asymptotic behaviour. The moments of displacement and the position-position auto-correlation functions of the LLg$^+$ agree with those of the LLg. For the LLg there are theoretical results for the moments of displacement (Burioni et al., 2010), and they can be matched with the findings for the SM (Table 1 and (Salari et al., 2015)). In contrast, there are no analytical results available for the time dependent position-position auto-correlation function. Time correlations in anomalous transport constitute by and large an open problem.

Our numerical results indicate that there also is an equivalence of the asymptotic scalings of the position-position auto-correlation functions of the SM and the LLg$^+$. As established in Salari et al. (2015) for the equivalence of moments, the agreement is based on the matching of the transport exponent, γ. Hence, the parameters α and β obey the relation Eq. (42). No

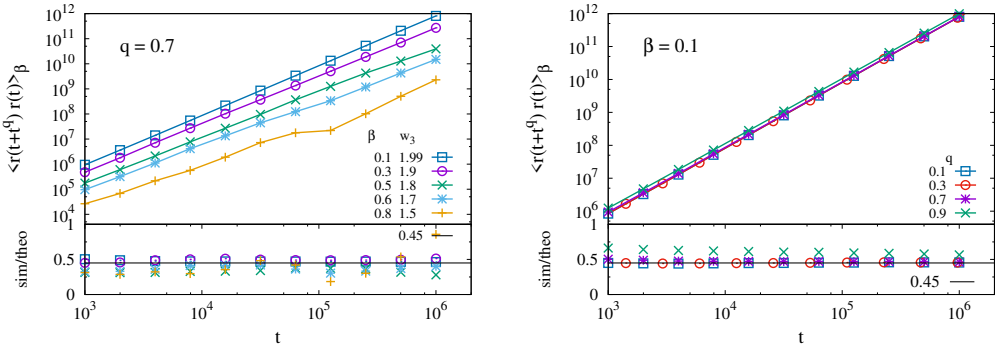

(a) Varying β for fixed $q = 0.7$.

(b) Varying q for fixed $\beta = 0.1$.

Figure 4: Log-log plot of the correlation $\langle r(t)r(t+t^q)\rangle_\beta$ as a function of time t for various values of β and of q. The respective values for β and q are specified in the figure legends. Figure 4a also specifies the values for the exponents w_3 that provide the best fit to the data. Also in this case the dependence of w_3 agrees faithfully with the expected value $\gamma(\beta)$ that has been provided in Table 1. Further, the approach of the data towards the solid line in the bottom panel demonstrates again that Eq. (50a) provides a faithful asymptotic scaling, with $C_3 = 0.45$.

further parameters are adjusted to also achieve the matching of the auto-correlation function.[5] As β increases, the agreement between the numerical data and the proposed expressions for the asymptotic scaling of the auto-correlation function becomes less convincing. Presently, it is not clear whether the correspondence only holds for small values of β, or whether the emerging discrepancies are due to the increasing difficulty of obtaining good statistics with growing β. This issue goes beyond the scope of the present work. It will be investigated in a future paper.

We emphasise that the agreement of the moments and the time-dependent auto-correlation for the displacement hold in spite of the fact that the SM and the LLg$^+$ exhibit entirely different dynamics. Intuition on the properties of the SM and of the LLg$^+$ can be obtained by observing the relative motion of two points. For the SM, take $\hat{\mathbf{x}} = (x, 0)$ and $\hat{\mathbf{y}} = (y, 0)$ in $\widehat{M}$. There are two possible cases: either there exists an interval $(\ell^+_{j-1}(\alpha), \ell^+_j(\alpha)]$ such that $x, y \in (\ell^+_{j-1}(\alpha), \ell^+_j(\alpha)]$, or such an interval does not exist.

1. When the interval exists the coarse-grained trajectories of $\hat{\mathbf{x}}$ and $\hat{\mathbf{y}}$, namely $x(n) := \pi_{\mathbb{Z}}(S^n_\alpha(\hat{\mathbf{x}}))$ and $y(n) := \pi_{\mathbb{Z}}(S^n_\alpha(\hat{\mathbf{y}}))$, coincide for all times n: particles sharing this property never separate. For all times they remain at a the initial distance from each other.

2. Otherwise, take $x \in (\ell^+_{\overline{m}_\alpha(x)-1}(\alpha), \ell^+_{\overline{m}_\alpha(x)}(\alpha)]$ and $y \in (\ell^+_{\overline{m}_\alpha(y)-1}(\alpha), \ell^+_{\overline{m}_\alpha(y)}(\alpha)]$, with $(\ell^+_{\overline{m}_\alpha(x)-1}(\alpha), \ell^+_{\overline{m}_\alpha(x)}(\alpha)] \cap (\ell^+_{\overline{m}_\alpha(y)-1}(\alpha), \ell^+_{\overline{m}_\alpha(y)}(\alpha)] = \varnothing$ and $x < y$, which implies $\overline{m}_\alpha(x) < \overline{m}_\alpha(y)$. This means that the two points have the same coarse grained trajectory up to time $\overline{m}_\alpha(x)$, when $\hat{\mathbf{x}}$ enters its periodic orbit, while $\hat{\mathbf{y}}$ continues its ballistic motion up to time $\overline{m}_\alpha(y)$. At times larger than $\overline{m}_\alpha(y)$, the distance between the two particles equals either $\overline{m}_\alpha(y) - \overline{m}_\alpha(x)$ or $\overline{m}_\alpha(y) - \overline{m}_\alpha(x) \pm 1$. For all points with $x, y \in (0, 1)$, the distance becomes periodic after a finite initial transient.

Consequently, any function of any finite number of points, evaluated along a trajectory of the SM, turns periodic in a finite time. This situation is totally different from that of the

[5] Actually, we did not take the parameters suggested by the relation (42) for the equivalence of the moments, in order to find the data collapse for the correlations. On the contrary, we looked for the parameters that provide the best data collapse for the correlations, and we found that their values are indeed with good accuracy those given by Eq. (42).

LLg^+, whose nature renders the distance between any two particles, hence any function of a finite number of positions, stochastic.

We conclude that position-position auto-correlations do not distinguish the SM and the LLg^+. This equivalence can be used to indirectly investigate some of the elusive properties of the LLg^+. Given the non-physical features of the SM this may appear puzzling. However, from the perspective of statistical mechanics one could also argue that it is not surprising. After all, in statistical mechanics the details of the microscopic dynamics of large systems usually do not strongly affect the behaviour of physically relevant macroscopic quantities. The latter can thus agree even for systems with vastly different microscopic dynamics. This observation lies at the heart of the success of highly idealized models in describing complex phenomena; even simple models may capture the essential ingredients determining the behaviour of a selected and limited number of observables. Theoretical models for critical phenomena and universality constitute examples of this fact (Simon, 1993; Gallavotti, 1999; Kadanoff, 2000; Chibbaro et al., 2014). However, in general, one does not know how far equivalence can go, and which properties it may concern, especially for far-from-equilibrium transient dynamics with anomalous transport behaviour. For instance, even for thermodynamic particle systems the Local Thermodynamic Equilibrium condition, required for the existence of the thermodynamic fields, is quite a sophisticated property whose underpinning requires a long sequence of microscopic conditions, as expressed by Spohn (1991): *"The propagation of local equilibrium in time, if true, is a deep and highly non-obvious property of a system of many particles governed by Newton equations of motion"*. For the position auto-correlations of the SM and the LLg or the LLg^+a direct investigation was therefore required. The conclusion is that the SM can be used to indirectly investigate the LLg^+: agreement of transport exponents implies matching of the two-point auto-correlation functions. Thus, the transport exponent might be a kind of counterpart of critical exponents, suitable for the characterisation of transport phenomena: analogously to critical exponents, they afford a coarse but equally useful description of the systems at hand.

Acknowledgements

The authors are grateful to the computational resources provided by HPC@POLITO, a project of Academic Computing within the Department of Control and Computer Engineering at the Politecnico di Torino (`http://hpc.polito.it`). C.G. acknowledges financial support from "Fondo di Ateneo per la Ricerca 2016" under the project "Sistemi stocastici e deterministici su strutture spaziali discrete, grafi e loro proprietà strutturali", Università di Modena e Reggio Emilia. J.V. is grateful for the appointment as a Distinguished Visiting Professor at the Department of Mathematical Sciences of the Politecnico di Torino.

A Contributions to the Slicer Correlation Function

In this Appendix we compute the asymptotics of the sums defined in Eqs. (19a) and (30). By Taylor expansion we have:

$$\Delta_k(\alpha) = \ell_k^+(\alpha) - \ell_{k-1}^+(\alpha) = \frac{\alpha}{k^{\alpha+1}} \left(1 - \tilde{c}(\alpha)\,\frac{1}{k} + O\left(\frac{1}{k^2}\right)\right), \tag{51a}$$

where

$$\tilde{c}(\alpha) = (1+\alpha)\left(2^{\frac{1}{\alpha}} - \frac{1}{2}\right) > 0 \qquad \text{with} \quad \alpha > 0\,. \tag{51b}$$

Then, the sum in Eq. (19a) can be written as:

$$\sum_{k=1}^{n-1} k^2\,\Delta_k(\alpha) = \sum_{k=1}^{n-1} \frac{\alpha}{k^{\alpha-1}}\,(1 - f(k))\,, \tag{52a}$$

where

$$f(k) := \tilde{c}(\alpha)\,\frac{1}{k} + O\left(\frac{1}{k^2}\right)\,. \tag{52b}$$

The previous equation implies the existence of an integer n_0 such that:

$$\frac{1}{2}\,\tilde{c}(\alpha)\,k^{-1} < f(k) < \frac{3}{2}\,\tilde{c}(\alpha)\,k^{-1} \qquad \text{for} \quad k > n_0\,. \tag{53}$$

Then, for $m > n_0$ we have:

$$\sum_{k=1}^{n-1} k^2 \Delta_k(\alpha) = \sum_{k=1}^{n-1} \frac{\alpha}{k^{\alpha-1}} - \sum_{k=1}^{n_0} \frac{\alpha\, f(k)}{k^{\alpha-1}} - \sum_{k=n_0}^{n-1} \frac{\alpha\, f(k)}{k^{\alpha-1}}, \tag{54a}$$

where

$$\frac{1}{2}\tilde{c}(\alpha) \sum_{k=n_0}^{n-1} \frac{1}{k^\alpha} \le \sum_{k=n_0}^{n-1} \frac{f(k)}{k^{\alpha-1}} \le \frac{3}{2}\,\tilde{c}(\alpha) \sum_{k=n_0}^{n-1} \frac{1}{k^\alpha}\,. \tag{54b}$$

Therefore, the last sum in Eq. (54a) is of the order of $\sum_{k=n_0}^{n-1} k^{-\alpha}$, for $m \to \infty$. We evaluate the scaling of the two other terms based on the Euler-Maclaurin sum formula:

Lemma 15 (Euler-Maclaurin sum formula) *For a smooth function $g(x)$, the full asymptotic behaviour of*

$$G(n) = \sum_{k=0}^{n} g(k), \tag{55}$$

is given by

$$G(n) \sim \frac{1}{2}g(n) + \int_0^n g(t)\,dt + C + \sum_{j=1}^{\infty} (-1)^{j+1} \frac{B_{j+1}}{(j+1)!} g^{(j)}(n) \qquad \textit{as} \quad n \to \infty\,. \tag{56}$$

Here C is a constant depending on g, and B_j are the Bernoulli numbers.

Specifically, for $g(k) = k^p$ and $p \neq -1$ one has

$$\sum_{k=0}^{m} k^p \sim \frac{m^{p+1}}{p+1} + \frac{1}{2}m^p + C + \sum_{j=1}^{\infty} (-1)^{j+1} \frac{B_{j+1}}{(j+1)!} \prod_{\ell=0}^{j-1} (p-\ell)\, m^{p-j} \qquad \textit{as} \quad m \to \infty \tag{57a}$$

while $p = -1$ entails:

$$\sum_{k=1}^{m} k^{-1} \sim \ln m + C + \frac{1}{2\,m} - \frac{B_2}{2\,m^2} - \frac{B_4}{4\,m^4} - \ldots \qquad \textit{as} \quad m \to \infty\,. \tag{57b}$$

Proof. See for instance Bender and Orszag (1979). □

For $\alpha > 2$ Eq. (57a) entails that the sum Eq. (52a) converges to a finite value, as reported in Eq. (19a).

For $\alpha = 2$ Eq. (57b) provides

$$\sum_{k=1}^{n-1} k^2\, \Delta_k(\alpha) \sim 2\alpha\, \ln n \qquad \text{for} \quad \alpha = 2\,, \tag{58a}$$

i.e. the logarithmic scaling reported in Eq. (19a).

For $0 < \alpha < 2$ we have that the two sums depending on m in Eq. (54a) diverge:

$$\sum_{k=1}^{m} \frac{\alpha}{k^{\alpha-1}} \sim \frac{\alpha}{2-\alpha} m^{2-\alpha}\,, \qquad \sum_{k=m_0}^{m} \frac{\alpha f(k)}{k^{\alpha-1}} = O(m^{1-\alpha}) \qquad \text{as} \quad m \to \infty\,,$$

where the second sum is estimated using Eq. (54b). From Eq. (54a), we then obtain

$$\sum_{k=1}^{n-1} k^2 \Delta_k(\alpha) \sim \frac{\alpha}{2-\alpha}\, n^{2-\alpha} \qquad \text{for} \quad 0 < \alpha < 2\,. \tag{58b}$$

This concludes the derivation of Eq. (19a).

Equation (30) can be evaluated by the same line of argumentation. Using Eq. (51a), the sum in Eq. (30) yields:

$$\sum_{k=1}^{n} k\, \Delta_k(\alpha) = \frac{\alpha}{1+\alpha} \sum_{k=1}^{n} \frac{1+\alpha}{k^\alpha}\, (1 - f(k))\,. \tag{59}$$

This is the same expression as Eq. (52a), except for the constant factor in front of the sum and substituting $\alpha - 1 \to \alpha$ in the sum. Consequently, according to Eq. (57a) the sum takes a finite value for $\alpha > 1$. Moreover, introducing the substitutions into Eq. (58b) yields

$$\sum_{k=1}^{n} k\, \Delta_k(\alpha) \sim \frac{\alpha}{1+\alpha}\, \frac{1+\alpha}{1-\alpha}\, n^{1-\alpha} = \frac{\alpha}{1-\alpha}\, n^{1-\alpha} \qquad \text{for} \quad 0 < \alpha < 1\,, \tag{60}$$

which is the non-trivial scaling reported in Eq. (30). Analogously, the logarithmic scaling in Eq. (30) is obtained from Eq. (58a), where the right-hand-side must be evaluated for $\alpha = 1$ due to the substitution. This concludes the derivation of Eq. (30).

References

E. Aghion, D. A. Kessler, and E. Barkai. Large fluctuations for spatial diffusion of cold atoms. *Phys. Rev. Lett.*, 118:260601, 2017.

E. Barkai and V. Fleurov. Stochastic one-dimensional Lorentz gas on a lattice. *J. Stat. Phys.*, 96:325, 1999.

E. Barkai, V. Fleurov, and J. Klafter. One-dimensional stochastic Lévy-Lorentz gas. *Phys. Rev. E*, 61:1164, 2000.

C. M. Bender and S. A. Orszag. *Advanced mathematical methods for scientist and engineers*. McGraw-Hill, Singapore, 1979.

A. Bianchi, G. Cristadoro, M. Lenci, and M. Ligabò. Random walks in a one-dimensional Lévy random environment. *J. Stat. Phys.*, 163:22–40, 2016. doi: 10.1007/s10955-016-1469-0. arxiv/1411.0586v2.

R. Burioni, L. Caniparoli, and A. Vezzani. Lévy walks and scaling in quenched disordered media. *Phys. Rev. E*, 81:060101(R), 2010.

F. Cecconi, D. del Castillo-Negrete, M. Falcioni, and A. Vulpiani. The origin of diffusion: The case of non chaotic systems. *Physica D*, 180:129, 2003.

S. Chibbaro, L. Rondoni, and A. Vulpiani. *Reductionism, Emergence and Levels of Reality. The Importance of Being Borderline*. Springer Verlag, Heidelberg, 2014.

P. Collet, M. Courbage, S. Métens, A. Neishtadt, and G. Zaslavsky, editors. *Lecture on Transport and Front Propagation*, Nato Science Series II, Heidelberg, 2005. Springer. doi: 10.1007/1-4020-2947-0. Proceedings of the NATO Advanced Study Institute on International Summer School on Chaotic Dynamics and Transport in Classical and Quantum Systems, Cargèse, Corsica, 18 - 30 August 2003.

S. Denisov, J. Klafter, and M. Urbakh. Dynamical heat channels. *Phys. Rev. Lett.*, 91: 194301, 2003.

C. P. Dettmann and E. G. D. Cohen. Microscopic chaos and diffusion. *J. Stat. Phys.*, 101: 775, 2000.

G. Gallavotti. *Statistical Mechanics*. Springer Verlag, Berlin, 1999.

P. Gaspard. *Chaos, scattering and statistical mechanics*. Cambridge University Press, Cambridge, 2005.

O. G. Jepps and L. Rondoni. Thermodynamics and complexity of simple transport phenomena. *J. Phys. A: Math. Gen.*, 39:1311, 2006.

O. G. Jepps, S. K. Bathia, and D.J. Searles. Wall mediated transport in confined spaces: exact theory for low density. *Phys. Rev. Lett.*, 91:126102, 2003.

L. P. Kadanoff. *Statistical Physics: statics, dynamics and renormalization*. World Scientific, Singapore, 2000.

J. Klafter, S. C. Lim, and R. Metzler. *Fractional Dynamics: Recent Advances*. World Scientific, Singapore, 2012.

R. Klages. *Microscopic chaos, fractals and transport in nonequilibrium statistical mechanics*, volume 24 of *Advanced Series in Nonlinear Dynamics*. World Scientific, Singapore, 2007.

R. Klages, G. Radons, and I.M. Sokolov, editors. *Anomalous Transport: Foundations and Applications*. Wiley-VCH, Weinheim, 2008.

B. Li, J. Wang, L. Wang, and G. Zhang. Anomalous heat conduction and anomalous diffusion in nonlinear lattices, single walled nanotubes, and billiard gas channels. *Chaos*, 15:015121, 2005.

L. Rondoni and E. G. D. Cohen. Gibbs entropy and irreversible thermodynamics. *Nonlinearity*, 13:1905, 2000.

D. Ruelle. Differentiation of SRB states. *Comm. Math. Phys.*, 187:227, 1997.

D. Ruelle. General linear response formula in statistical mechanics, and the fluctuation dissipation theorem far from equilibrium. *Phys. Lett. A*, 245:220, 1998.

L. Salari, L. Rondoni, C. Giberti, and R. Klages. A simple non-chaotic map generating subdiffusive, diffusive, and superdiffusive dynamics. *Chaos*, 25:073113, 2015.

B. Simon. *The statistical mechanics of lattice gases*. Princeton University Press, Princeton, 1993.

I. M. Sokolov. Models of anomalous diffusion in crowded environments. *Soft Matter*, 8:9043, 2012.

H. Spohn. *Large Scale Dynamics of Interacting Particles*. Texts and Monographs in Physics. Springer Verlag, Heidelberg, 1991.

G. M. Zaslavsky. Chaos, fractional kinetics, and anomalous transport. *Phys. Rep.*, 371:461, 2002.